Eur. J. Mech. B - Fluids 20 (2001) 751–770

S0997-7546(01)01146-3/FLA

Transverse-roll global modes in a Rayleigh–Bénard–Poiseuille system with streamwise variable heating

Philippe Carrière [a,*], Peter A. Monkewitz [b]

[a] *Laboratoire de Mécanique des Fluides et d'Acoustique, UMR CNRS 5509, Ecole Centrale de Lyon-Université Claude Bernard Lyon I, BP163, 69131 Ecully cedex, France*

[b] *Laboratoire de Mécanique des Fluides, Ecole Polytechnique Fédérale de Lausanne, CH-1015 Lausanne, Switzerland*

(Received 10 November 2000; revised 18 May 2001; accepted 24 May 2001)

Abstract – The effect of a spatially inhomogeneous heating of the bottom wall in Rayleigh–Bénard–Poiseuille convection is studied for slow streamwise variations of the temperature profile. The problem is defined by the constant Reynolds number of the Poiseuille through flow, assumed to be low (typically $\leqslant 10$), the constant Prandtl number, and the spatial evolution of the Rayleigh number $\mathcal{R}(X)$, assumed to be subcritical everywhere except in a limited region around its single maximum $\mathcal{R}^{\mathrm{t}}$. In this initial study, all spanwise inhomogeneities such as side walls or spanwise variable heating are neglected to obtain two-dimensional (transverse roll) global mode solutions by means of WKBJ asymptotics. The resulting frequency selection yields, at leading order, a global mode frequency equal to the local absolute frequency ω^{t} at the streamwise location where the Rayleigh number is maximum, with higher-order corrections for non-parallelism. These allow the determination of critical values of $\mathcal{R}^{\mathrm{t}}$ for global instability as a function of the profile of the local Rayleigh number $\mathcal{R}(X)$ and of Prandtl and Reynolds numbers. © 2001 Éditions scientifiques et médicales Elsevier SAS

global modes / mixed convection

1. Introduction

Over the last two decades, the stability properties of non-parallel flows have received increasing attention as many flows of practical importance are non-parallel, in particular open flows such as mixing layers, jets, wakes and boundary layers. While the stability of strongly non-parallel flows can only be investigated numerically, analytical progress has been made for weakly non-parallel flows which evolve slowly on the scale of a typical instability wave length. In this case, the temporal instability modes of a weakly non-parallel flow, commonly termed global modes [1], have been related to its local stability properties, in particular to the presence of local convective and absolute instability [2]. When a sufficiently large region of locally absolute instability exists, it is generally possible to construct unstable (time-amplified or self-sustained) global modes by means of WKBJ analysis (other types of global modes may exist [3,4], but will not be discussed in the following). In the course of such analyses, a selection criterion for the complex frequency naturally appears [5] when requiring boundedness of solutions at upstream and downstream infinity. In practice, the frequency selection is obtained from the matching of subdominant upstream and downstream WKBJ approximations through turning points where the latter break down.

Such approaches have been successfully applied to model equations [6,2] as well as to real flows, such as Taylor vortex flow in the gap between concentric spheres [7] or shear flows [8]. In thermal convection, the influence of spatially inhomogeneous boundary conditions have been studied in the Rayleigh–Bénard system

* Correspondence and reprints.
E-mail address: carriere@mecaflu.ec-lyon.fr (P. Carrière).

without through flow for instance by Walton [9], who considered a layer with slowly increasing depth, and Rees [10], who analyzed convection in a slab of porous medium with a spatially modulated wall temperature. The problem closest to the subject of this paper is the fluid layer with a slow downstream increase of the temperature difference between top and bottom walls combined with through-flow, which has been investigated by Walton [11]. He used an envelope formalism restricted to small Reynolds and small supercritical Rayleigh numbers, i.e. to the vicinity of the onset of convective instability. Since the temperature difference in Walton's analysis is unbounded at downstream infinity, the amplitude of the convection rolls shows the same behaviour. Nevertheless, the analysis predicts a downstream shift of the neutral point, i.e. the location where rolls start to grow, relative to the neutral point predicted from standard locally parallel analysis, a phenomenon that will also be observed in our study (see the discussion related to our *figure 8*).

In the present paper, a two-dimensional horizontal channel heated from below with low Reynolds number uni-directional through-flow is analyzed. The non-parallel effects are introduced into this so-called Rayleigh–Bénard–Poiseuille system by a differential heating which varies slowly (on the scale of the channel height) in the streamwise direction. By choosing a more general streamwise inhomogeneity than Walton [9], the limitations of his analysis with respect to the shape of the thermal inhomogeneity and the magnitude of the Reynolds number are overcome. Specifically, by placing stable regions far up- and down-stream, the linear global mode problem with homogeneous boundary conditions at up- and down-stream infinity is well posed, i.e. the global mode amplitude remains bounded over the entire doubly infinite domain and problems with causality are avoided (see e.g. the discussion in Hunt and Crighton [12]). Hence, it will be possible to determine the critical Rayleigh number as a function of Reynolds number for the temporal growth of a global mode as well as the frequency at which such a mode is synchronized over the entire domain.

The fact of using a doubly infinite domain in the stream-wise direction does not appear to be overly artificial, since the effect of the channel inlet in an experiment, and to a lesser degree of the outlet, on the global mode can be minimized by placing them in zones which are stable with respect to the thermal convective instability. Furthermore, in order to focus on thermal convective (Rayleigh–Bénard) instability modes, the Reynolds number for the following investigation is chosen sufficiently low (typically below 10) to exclude shear driven instabilities. Hence, the non-parallel effects associated with the development of the Poiseuille velocity profile at the channel entrance can be neglected, since this development length is very short (a few channel heights) and assumed to be in a stable region. This is in contrast with isothermal flow in a two-dimensional channel of constant height where the only non-parallel effects are associated with the development of the velocity profile at the channel entrance.

The choice of the present system is motivated by the desire of moving away from the traditional analysis of the highly idealized spatially homogeneous flow towards more realistic situations with imperfect temperature boundary conditions, i.e. with 'hot spots'. Since the spatially homogeneous Rayleigh–Bénard–Poiseuille flow is known to exhibit a transition from convective to absolute instability [13,14], it is also considered to be an interesting prototypical system for future experimental investigations of global modes. It is clear that the present two-dimensional analysis, which excludes any spanwise inhomogeneity such as walls or spanwise non-uniform heating, can only be a first but necessary step towards understanding the stability properties of more realistic, fully three-dimensional systems in which convection modes other than rolls may dominate.

As will be shown in the following sections, the analysis is relatively straightforward, at least in the present two-dimensional situation, as the only spatially (slowly) evolving parameter is the local Rayleigh number, while the Prandtl and Reynolds numbers remain constant. The characterization of the most amplified global mode is thus obtained by building on our previous locally parallel stability analysis [14]. The paper is organized as follows. Section 2 is devoted to the establishment of the non-parallel base flow in terms of multiple scale approximations. The next section 3 is devoted to the WKBJ approximation of the global modes and the

identification of WKBJ turning points. Provided the streamwise varying local Rayleigh number has a unique maximum within the doubly infinite flow domain and is sufficiently low (assumed subcritical in this paper) at upstream and downstream infinity, the global frequency is determined by a double turning point at the streamwise location where the differential heating is maximum. This double turning point region, through which the upstream and downstream WKBJ approximations are matched, is analyzed in section 4. Finally, results for a Gaussian streamwise variation of the Rayleigh number are presented and discussed in section 5.

2. Base flow

We consider a two-dimensional layer of fluid, of depth h in the vertical z-direction, of infinite extent in the horizontal x-directions, in which a laminar mean through-flow is forced by maintaining a suitable constant pressure gradient in the x-direction. The origin of the coordinates are taken at the center of the fluid layer and the length scale for non-dimensionalization is h. The fluid flow is intended to satisfy the usual conservation equation under the Boussinesq approximation. The mean velocity and pressure field are thus given by:

$$\mathbf{U}_p = \tilde{U}_p(z)\mathbf{e}_x = \left(1 - 4z^2\right)\mathbf{e}_x, \tag{1}$$

$$\Pi_p = -\frac{8}{R}x, \tag{2}$$

where we used the maximum of the dimensional Poiseuille profile U_m for scaling the velocity so that the Reynolds number is:

$$R = \frac{U_m h}{\nu}, \tag{3}$$

ν being the kinematic viscosity of the fluid. On the upper wall bounding the fluid, the temperature is assumed to be at a constant value T_r relative to which temperatures are defined: in non-dimensional form, we thus have:

$$T = 0 \quad \text{at } z = 1/2. \tag{4}$$

On the lower wall, the dimensional temperature T_*^+ is assumed to depend slowly on the coordinate in the x-direction. Denoting g, α and K the gravitational acceleration, the thermal expansion coefficient and the thermal diffusivity respectively, the quantity $g^{-1}\alpha^{-1}h^{-3}\nu K$ is used as the scale for temperature differences. Introducing $X = \varepsilon x$ ($\varepsilon \ll 1$), as the slow non-dimensional coordinate in the x-direction, the boundary condition thus becomes:

$$T = \mathcal{R}(X) \quad \text{at } z = -1/2, \tag{5}$$

where $\mathcal{R}(X)$ is the local Rayleigh number defined as:

$$\mathcal{R}(X) = \frac{g\alpha h^3 (T_*^+(X) - T_r)}{\nu K}. \tag{6}$$

Considering the slow dependence of the lower wall temperature on X, the resulting steady, weakly non-parallel base flow is obtained by a multiple scale expansion. The deviation $\mathbf{U}_b$ and Π_b from the Poiseuille velocity $\mathbf{U}_p$ and pressure Π_p, together with the base temperature T_b are expanded as [1]:

[1] Note that velocity is scaled using K/h and pressure using $\rho\nu K h^{-2}$.

$$\Pi_b(X,z) = \Pi_0(X,z) + \varepsilon\Pi_1(X,z) + \varepsilon^2\Pi_2(X,z) + \mathrm{O}(\varepsilon^3), \tag{7}$$

$$\mathbf{U}_b(X,z) = \mathbf{U}_0(X,z) + \varepsilon\mathbf{U}_1(X,z) + \varepsilon^2\mathbf{U}_2(X,z) + \mathrm{O}(\varepsilon^3), \tag{8}$$

$$T_b(X,z) = T_0(X,z) + \varepsilon T_1(X,z) + \varepsilon^2 T_2(X,z) + \mathrm{O}(\varepsilon^3). \tag{9}$$

At leading order, the following set of equations is obtained:

$$\partial_z(\mathbf{U}_0\cdot\mathbf{e}_z) = 0, \tag{10}$$

$$P^{-1}(\mathbf{U}_0\cdot\mathbf{e}_z)\partial_z\mathbf{U}_0 + R\tilde{U}_p'(\mathbf{U}_0\cdot\mathbf{e}_z)\mathbf{e}_x + \partial_z\Pi_0\mathbf{e}_z - T_0\mathbf{e}_z - \partial_z^2\mathbf{U}_0 = 0, \tag{11}$$

$$(\mathbf{U}_0\cdot\mathbf{e}_z)\partial_z T_0 - \partial_z^2 T_0 = 0, \tag{12}$$

where $P = \nu/K$ is the Prandtl number and $\tilde{U}_p'$ is the z-derivative of $\tilde{U}_p$, together with boundary conditions:

$$\mathbf{U}_0(X,\pm 1/2) = 0, \qquad T_0(X,1/2) = 0, \qquad T_0(X,-1/2) = \mathcal{R}(X). \tag{13}$$

Locally, this problem is identical to the parallel one so that leading order solutions only depend parametrically on X through the local Rayleigh number $\mathcal{R}(X)$. They are easily obtained as:

$$\Pi_0 = \mathcal{R}(X)\tilde{\Pi}_0(z), \qquad \mathbf{U}_0 = 0, \qquad T_0 = \mathcal{R}(X)\tilde{T}_0(z),$$
$$\text{with } \tilde{\Pi}_0 = -\frac{1}{8}\left[(1-2z)^2 + C_1\right] \text{ and } \tilde{T}_0(z) = \frac{1}{2}(1-2z), \tag{14}$$

where the constant C_1 will be determined at higher order such as to enforce incompressibity.

At the next order $\mathrm{O}(\varepsilon)$, the following set of linear, inhomogeneous, equations is obtained:

$$\partial_z(\mathbf{U}_1\cdot\mathbf{e}_z) = 0, \tag{15}$$

$$R\tilde{U}_p'(\mathbf{U}_1\cdot\mathbf{e}_z)\mathbf{e}_x + \partial_z\Pi_1\mathbf{e}_z - T_1\mathbf{e}_z - \partial_z^2\mathbf{U}_1 = -\mathcal{R}'(X)\tilde{\Pi}_0, \tag{16}$$

$$\mathcal{R}(X)\tilde{T}_0'(\mathbf{U}_1\cdot\mathbf{e}_z) - \partial_z^2 T_1 = -\mathcal{R}'(X)RP\tilde{U}_p\tilde{T}_0, \tag{17}$$

with homogeneous boundary conditions for $\mathbf{U}_1$ and T_1 on both horizontal walls. The solutions are thus of the form:

$$\Pi_1 = \mathcal{R}'(X)\tilde{\Pi}_1(z), \qquad \mathbf{U}_1 = \mathcal{R}'(X)\tilde{\mathbf{U}}_1(z), \qquad T_1 = \mathcal{R}'(X)\tilde{T}_1(z), \tag{18}$$

$\tilde{U}_1$ and $\tilde{T}_1$ are then obtained as:

$$\tilde{\mathbf{U}}_1(z) = \tilde{U}_1(z)\mathbf{e}_x, \quad \text{with } \tilde{U}_1(z) = \frac{1}{384}(1-4z^2)(4z^2 - 8z + 7 + 6C_1), \tag{19}$$

$$\tilde{T}_1(z) = -\frac{RP}{480}(1-4z^2)(24z^3 - 20z^2 - 14z + 25), \tag{20}$$

while $\tilde{\Pi}_1(z)$ (not required for the following) can be determined from $\tilde{\Pi}_1' = \tilde{T}_1$.

Using the continuity equation at order $\mathrm{O}(\varepsilon^2)$:

$$\partial_z(\mathbf{U}_2\cdot\mathbf{e}_z) = -\mathcal{R}''(X)\tilde{U}_1. \tag{21}$$

Together with the no slip condition, the constant C_1 in equations (14) and (19) is finally obtained as:

$$C_1 = -\frac{6}{5}. \tag{22}$$

3. WKBJ approximation for the 2-D perturbation problem

3.1. Perturbation equations

The linear stability analysis consists of studying the evolution of a small 2-D perturbation $\mathbf{v} = [p(X, z, t), \mathbf{u}(X, z, t), \theta(X, z, t)]$ around the base solution $[\Pi_b, \mathbf{U}_b, T_b]$ determined in the preceding section, where the perturbation is written as a vector containing the disturbance pressure p, velocity vector $\mathbf{u}$, and temperature θ.

If the base flow was parallel, i.e. X-independent, the analysis yields in standard fashion an infinite set of eigenvalues corresponding to plane waves with constant wave number k. For the present X-dependent base state, a global mode analysis needs to be performed to identify temporally amplified, synchronized modes on the entire flow domain. This global mode analysis can be carried out in the framework of the WKBJ approximation, if the streamwise evolution of the base flow is slow, as assumed ($\varepsilon \ll 1$). Following Soward and Jones [7], Huerre, Monkewitz, Le Dizes [2,8,3] and others, the WKBJ approximation for a perturbation wave of frequency ω, corresponding to transverse convection rolls, can be expanded as:

$$\mathbf{v}(X, z, t) = \big(\mathbf{v}_0(z; X, \omega) + \varepsilon \mathbf{v}_1(z; X, \omega) + \mathrm{O}(\varepsilon^2)\big) \exp\left(\frac{\mathrm{i}}{\varepsilon} \int k(X, \omega)\, \mathrm{d}X - \mathrm{i}\omega t\right). \tag{23}$$

Introducing the WKBJ approximation (23) into the governing equations, the following system of homogeneous linear equations for the leading order term of the perturbation, $\mathbf{v}_0 = [p_0, \mathbf{u}_0, \theta_0]$, is obtained

$$-\mathrm{i}k(\mathbf{u}_0 \cdot \mathbf{e}_x) - \partial_z(\mathbf{u}_0 \cdot \mathbf{e}_z) = 0, \tag{24}$$

$$-\mathrm{i}\omega P^{-1}\mathbf{u}_0 + \mathrm{i}kR\tilde{U}_p\mathbf{u}_0 + R\tilde{U}_p'(\mathbf{u}_0 \cdot \mathbf{e}_z)\mathbf{e}_x + (\mathrm{i}k\mathbf{e}_x + \mathbf{e}_z\partial_z)p_0 - \theta_0\mathbf{e}_z + \big(k^2 - \partial_z^2\big)\mathbf{u}_0 = 0, \tag{25}$$

$$-\mathrm{i}\omega\theta_0 + \mathrm{i}kRP\tilde{U}_p\theta_0 - \mathcal{R}(\mathbf{u}_0 \cdot \mathbf{e}_z) + \big(k^2 - \partial_z^2\big)\theta_0 = 0, \tag{26}$$

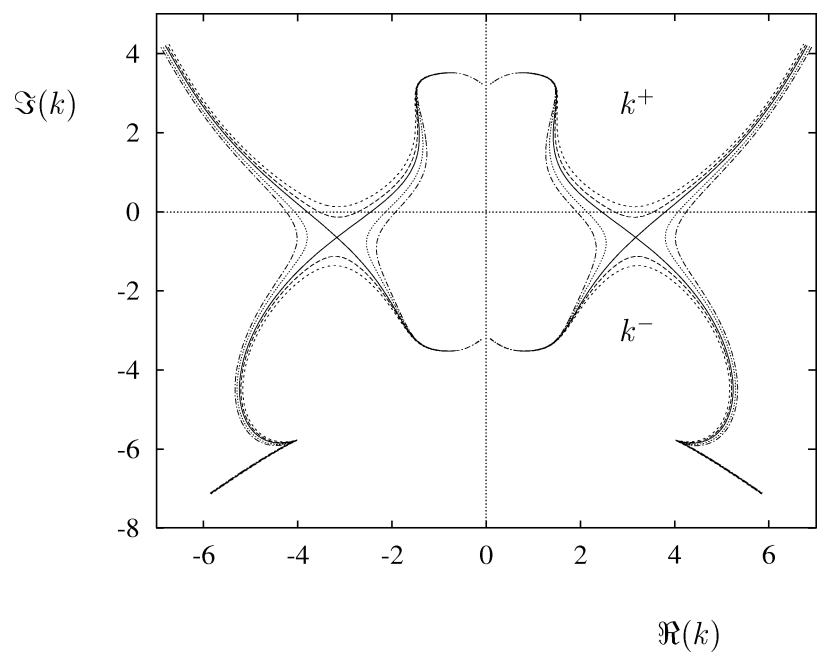

Figure 1. Spatial branches of the complex wavenumber k for different $\Im(\omega)$, Prandtl number $P = 7$, Reynolds number $R = 0.63$, and Rayleigh number $\mathcal{R}(X) = 1760$ (X fixed).

together with homogeneous boundary conditions on $\mathbf{u}_0$ and θ_0 at $z = \pm 1/2$. In the remainder of the paper, the equations (24)–(26) will be abbreviated as:

$$\mathcal{L}[\partial_z; \omega, X]A(X)\,\hat{\mathbf{v}}_0(z; \omega, X) = 0, \tag{27}$$

with the wave number k related to ω and X through the corresponding dispersion relation:

$$D[k, \omega, X] = 0. \tag{28}$$

Since the solution of (27) depends only parametrically on X through the local value of the Rayleigh number $\mathcal{R}(X)$, $\mathbf{v}_0$ has been factored into an unknown amplitude $A(X)$ and a suitably normalized 'structure function' $\hat{\mathbf{v}}_0$ (see appendices A and B). At any fixed station X, the wavenumber k represents spatial branches along which $\Re(\omega)$ varies, while $\Im(\omega)$ and X are held fixed, similar to the branches shown in [14]. A typical example is given in *figure 1*. Since, in the case of one-dimensional wave propagation, the spatial branches were found to move only little in the range of Rayleigh numbers $\mathcal{R}(X)$ of interest here [14], the spatial branches of *figure 1* can be regarded as representative for all stations X.

3.2. Global mode frequency selection

At this point ω in (23) is still a free parameter. The resolution of (27) only yields the spatial structure of a wave with an arbitrarily specified ω, evolving on the spatially varying base flow. This problem is commonly referred to as the signalling problem and has been studied, for instance, by Crighton and Gaster [15] in the jet.

To obtain a self-sustained global mode, particular values of ω must be sought for which no excitation source is required and $\Im(\omega) \geqslant 0$. Detailed discussions of the selection criteria for the global mode frequency ω_G are given in [8,3]. In the following, we just briefly summarize the salient features of the argument. The selection criterion for the global mode frequency arises from the physical requirement that global modes vanish in the limits $X \to \pm\infty$. In the present context, the following conditions on the control parameter $\mathcal{R}(X)$ is necessary:

$$\lim_{X\to\pm\infty} \mathcal{R}(X) < \mathcal{R}_c, \tag{29}$$

with $\mathcal{R}_c$ denoting the critical value for linear temporal instability of the parallel system. For simplicity, it is also assumed that $\mathcal{R}(X)$ has only one extremum, which is a maximum at the origin $X = 0$:

$$\mathcal{R}'(X = 0) = 0. \tag{30}$$

As shown by the authors mentioned above, most of the solutions of the form (23) are in fact unbounded in one of the limits $X \to \pm\infty$, and only situations in which the WKBJ approximation breaks down lead to global modes. Boundedness of the WKBJ approximation (23) in the limits $X \to \pm\infty$ requires that $\Im(k) < 0$ for $X \to -\infty$ and $\Im(k) > 0$ for $X \to +\infty$. Hence, for a given ω, one has to choose $k(\omega, X)$ on a branch k^- which is subdominant for $X < X^- < 0$, and on a branch k^+ which is subdominant for $X > X^+ > 0$:

$$\begin{aligned}\mathbf{v}(X, z, t) = {} & \big(A^{\pm}(X)\hat{\mathbf{v}}_0^{\pm}(z; \omega, X) + \varepsilon\mathbf{v}_1^{\pm}(X, z) + \mathrm{O}(\varepsilon^2)\big) \\ & \times \exp\left(\frac{\mathrm{i}}{\varepsilon}\int_0^X k^{\pm}(\omega, X)\,\mathrm{d}X - \mathrm{i}\omega\right) \quad \text{for } X \notin [X^-, X^+].\end{aligned} \tag{31}$$

The global frequency selection thus reduces to the problem of finding ω's for which the two branches k^- and k^+ can be smoothly matched across the WKBJ turning points and the associated Stokes line network in the

region $[X^-, X^+]$ [3,8]. In the present problem, considering the conditions (29) and (30) on the local Rayleigh number and the local behavior of spatial branches of the complex wavenumber k, two kind of WKBJ turning points, where $\partial_k\omega = 0$, i.e. where two k-branches coalesce, are possible: simple and double turning points. An example of the latter is shown in *figure 2*, where the two branches represented as solid lines coalesce at $X = 0$. We note that, since (28) depends only parametrically on X through the local Rayleigh number $\mathcal{R}(X)$, we can write

$$\partial_X\omega = \partial_{\mathcal{R}}\omega\mathcal{R}'(X), \tag{32}$$

where we have formally introduced a partial derivative with respect to $\mathcal{R}$ (at constant k), with the complete expression given in appendix B. Hence, $\partial_X\omega = 0$ at the origin $X = 0$ which is therefore a double turning point of the WKBJ approximation with a corresponding frequency ω^t.

The conditions (29) and (30) also allow to have two simple turning points, as illustrated by *figure 3*. This case is more complex (see for instance [3]) since it requires a conversion from the k^- branch to a combination of intermediate k^- and k^+ branches at the first turning point and another conversion to the k^+ branch at the second turning point, which has to be linked to the first turning point by a Stokes line (this is not the case in *figure 3* so that the analysis would have to be extended to the complex X-plane). Note however that, in the present context, two simple turning points at X^- and X^+ are only possible for $\Im(\omega) = 0$ if $\mathcal{R}(X^-) = \mathcal{R}(X^+)$ are equal to the critical value $\mathcal{R}_a$ for local absolute instability. Consequently, $\mathcal{R}(0) > \mathcal{R}_a$ and the global mode associated with the double turning point at $X = 0$ has a positive growth rate at leading order. Therefore, the following analysis is restricted to the case of a double turning point, for which the leading order global mode frequency is entirely determined by the conditions

$$\partial_k\omega = \partial_X\omega = 0, \tag{33}$$

satisfied for $\omega = \omega^t$ at $X = X^t = 0$.

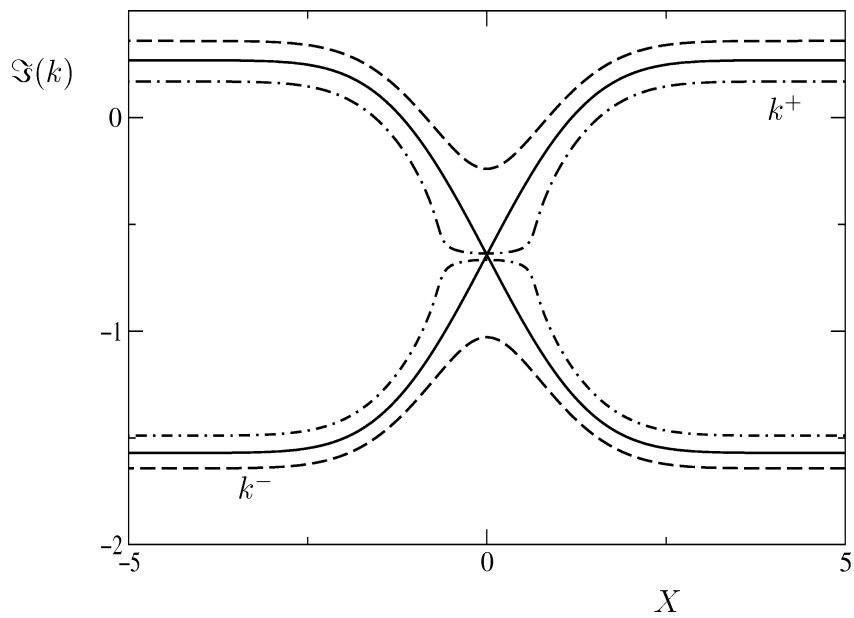

Figure 2. Imaginary part of the spatial branches $k(\omega, X)$ versus location X, at a fixed $\Re(\omega) = 12.058$ and $\Im(\omega) = 0$ (solid line), $\Im(\omega) > 0$ (dashed line) and $\Im(\omega) < 0$ (dot-dashed line). $P = 7$, $R = 0.63$ and $\mathcal{R}(X) = \mathcal{R}_\infty + (\mathcal{R}^t - \mathcal{R}_\infty)\exp(-X^2/2)$ with $\mathcal{R}_\infty = 1600$. The values of $\mathcal{R}(0) = \mathcal{R}^t = 1827.9 \approx \mathcal{R}_a$ and $\Re(\omega) \approx \Re(\omega_a)$ have been chosen so as to correspond to the convective-absolute transition.

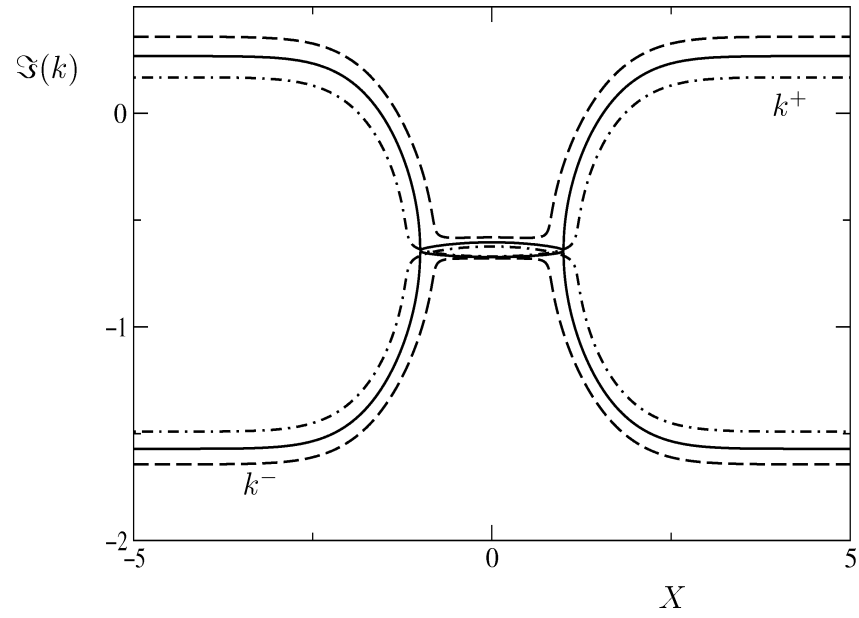

Figure 3. Same as in *figure 2*, except for: $\mathcal{R}^{\mathrm{t}} = 1975.8$ so as to have $\partial_k \omega = 0$ at $X = \pm 1$ for $\Im(\omega_0) = 0$.

The breakdown of the WKBJ approximation at the turning point requires a separate analysis of the $\mathrm{O}(\varepsilon^{1/2})$-neighborhood of $X^{\mathrm{t}} = 0$. The global mode frequency ω_{G} is thus expanded as

$$\omega_{\mathrm{G}} = \omega^{\mathrm{t}} + \varepsilon\omega_1 + \mathrm{O}(\varepsilon^{3/2}), \tag{34}$$

where ω_1 is determined by a solvability condition at order ε.

3.3. WKBJ solution to $\mathrm{O}(\varepsilon)$ *away from turning points*

At order $\mathrm{O}(\varepsilon)$, the inhomogeneous system of linear equations for $\mathbf{v}_1^{\pm} = (p_1^{\pm}, \mathbf{u}_1^{\pm}, \theta_1^{\pm})$ is:

$$\mathcal{L}\big[\partial_z; \omega^{\mathrm{t}}, X\big]\mathbf{v}_1^{\pm}(z; \omega^{\mathrm{t}}, X) = \mathcal{S}_1\mathbf{v}_0^{\pm}, \tag{35}$$

where the components of $\mathcal{S}_1\mathbf{v}_0^{\pm}$ read:

$$\begin{aligned}
\mathcal{S}_1\mathbf{v}_0^{\pm} = \big[&\partial_X A^{\pm}(\hat{\mathbf{u}}_0^{\pm}\cdot\mathbf{e}_x) + A^{\pm}(X)\partial_X(\hat{\mathbf{u}}_0^{\pm}\cdot\mathbf{e}_x),\ \partial_X A^{\pm}\big\{(2\mathrm{i}k^{\pm} - R\tilde{U}_p)\hat{\mathbf{u}}_0^{\pm} - \hat{p}_0^{\pm}\mathbf{e}_x\big\}\\
&+ A^{\pm}(X)\big\{\mathrm{i}\omega_1 P^{-1}\hat{\mathbf{u}}_0^{\pm} + \mathrm{i}\partial_X k^{\pm}\hat{\mathbf{u}}_0^{\pm} - \partial_X\hat{p}_0^{\pm}\mathbf{e}_x + (2\mathrm{i}k^{\pm} - R\tilde{U}_p)\partial_X\hat{\mathbf{u}}_0^{\pm}\\
&- \mathcal{R}'(X)P^{-1}\big(\mathrm{i}k^{\pm}\tilde{U}_1\hat{\mathbf{u}}_0^{\pm} + \tilde{U}_1'(\hat{\mathbf{u}}_0^{\pm}\cdot\mathbf{e}_z)\mathbf{e}_x\big)\big\},\ \partial_X A^{\pm}\big\{2\mathrm{i}k^{\pm} - RP\tilde{U}_p\big\}\hat{\theta}_0^{\pm}\\
&+ A^{\pm}(X)\big\{\mathrm{i}\omega_1\hat{\theta}_0^{\pm} + \mathrm{i}\partial_X k^{\pm}\hat{\theta}_0^{\pm} + (2\mathrm{i}k^{\pm} - RP\tilde{U}_p)\partial_X\hat{\theta}_0^{\pm} - \mathcal{R}'(X)\big(\mathrm{i}k^{\pm}\tilde{U}_1\hat{\theta}_0^{\pm}\\
&+ \tilde{T}_0(\hat{\mathbf{u}}_0^{\pm}\cdot\mathbf{e}_x) + \tilde{T}_1'(\hat{\mathbf{u}}_0^{\pm}\cdot\mathbf{e}_z)\big)\big\}\big]^{\mathrm{T}}.
\end{aligned} \tag{36}$$

Enforcing orthogonality condition between the right-hand side $S_1\mathbf{v}_0^{\pm}$ of (36) and the eigenfunctions of the adjoint problem corresponding to the eigenvalue $\mathrm{i}\overline{\omega}^{\mathrm{t}}$, yields the evolution equation for $A^{\pm}(X)$:

$$\partial_k\omega^{\pm}\partial_X A^{\pm} + A^{\pm}(X)\left(-\mathrm{i}\omega_1 + \frac{1}{2}\partial_k^2\omega^{\pm}\partial_X k^{\pm} + \eta_{k\omega}\partial_X\omega^{\pm} + \eta_{\varepsilon}\mathcal{R}'(X)\right) = 0. \tag{37}$$

The coefficients in (37) are detailed in appendix B.

For the later matching of the outer WKBJ-solution

$$A^{\pm}(X)\hat{\mathbf{v}}_0^{\pm}(z;\omega^{\mathrm{t}},X)\exp\left(\frac{\mathrm{i}}{\varepsilon}\int_0^X k^{\pm}(\omega^{\mathrm{t}},X)\,\mathrm{d}X-\mathrm{i}\omega_{\mathrm{G}}t\right) \tag{38}$$

and inner solution in the turning point region, the behavior of (38) as $X\to 0$ is required. With $A^{\pm}(X)$ given by

$$\frac{A^{\pm}(X)}{A_0^{\pm}}=\exp\left(-\int_0^X\frac{-\mathrm{i}\omega_1+\frac{1}{2}\partial_k^2\omega^{\pm}\partial_X k^{\pm}+\eta_{k\omega}\partial_X\omega^{\pm}+\eta_{\varepsilon}\mathcal{R}'(X)}{\partial_k\omega^{\pm}}\,\mathrm{d}X\right), \tag{39}$$

where all expressions are evaluated at $\omega=\omega^{\mathrm{t}}$, the required limiting behavior for $X\to 0$ is obtained in terms of the inner variable $\chi=\varepsilon^{1/2}x=\varepsilon^{-1/2}X$ as:

$$A_0\chi^{-2a}\exp\left(-\alpha^{1/2}\frac{\chi^2}{2}\right)\exp\left(\frac{\mathrm{i}}{\varepsilon^{1/2}}k^{\mathrm{t}}\chi-\mathrm{i}\omega_{\mathrm{G}}t\right)\hat{\mathbf{v}}_0^{\mathrm{t}}(z)+\mathrm{O}\left(\varepsilon^{1/2}\right). \tag{40}$$

In (40) the following abbreviations have been used:

$$\alpha=\partial_X^2\omega^{\mathrm{t}}\left(\partial_k^2\omega^{\mathrm{t}}\right)^{-1}, \tag{41}$$

$$\beta=-2\omega_1\left(\partial_k^2\omega^{\mathrm{t}}\right)^{-1}, \tag{42}$$

$$a=\frac{1}{4}\left(1+\frac{\beta}{\alpha^{1/2}}\right). \tag{43}$$

In (40)–(43) the superscript t indicates that the different functions have to be evaluated for $\omega=\omega^{\mathrm{t}}$ and $X=0$. Also, $\alpha^{1/2}$ stands for the root with positive real part:

$$\Re\left(\alpha^{1/2}\right)>0. \tag{44}$$

Details of the derivation of (40) are given in appendix C.

4. Analysis of the WKBJ double turning point at $X=0$

4.1. Base flow in the turning point region

In the vicinity of $X=0$, the appropriate inner variable is χ, already introduced above. First, the base flow is expressed in terms of χ as a Taylor expansion around $\chi=0$. Using (9), this yields the following expansion of the temperature field T_b, for instance:

$$T_b(\chi,z)=T_0(0,z)+\varepsilon^{1/2}\chi\,\partial_X T_0|_{X=0}+\varepsilon\left(\frac{\chi^2}{2}\partial_X^2 T_0|_{X=0}+T_1(0,z)\right)+\mathrm{O}\left(\varepsilon^{3/2}\right). \tag{45}$$

Evaluating T_0 and T_1 at $X=0$, and taking into account that $\mathcal{R}'(X=0)=0$, T_b is finally obtained as:

$$T_b(\chi,z)=\mathcal{R}^{\mathrm{t}}\tilde{T}_0+\varepsilon\frac{\chi^2}{2}\mathcal{R}''^{\mathrm{t}}\tilde{T}_0+\mathrm{O}\left(\varepsilon^{3/2}\right), \tag{46}$$

where $\mathcal{R}''^{\mathrm{t}} = \mathcal{R}''(X=0)$. Similarly, the base velocity and base pressure fields are approximated as:

$$\mathbf{U}_b(\chi, z) = \mathrm{O}(\varepsilon^{3/2}), \tag{47}$$

$$\Pi_b(\chi, z) = \mathcal{R}^{\mathrm{t}}\tilde{\Pi}_0 + \varepsilon\frac{\chi^2}{2}\mathcal{R}''^{\mathrm{t}}\tilde{\Pi}_0 + \mathrm{O}(\varepsilon^{3/2}). \tag{48}$$

4.2. Solution of the perturbation equations in the turning point region

The perturbation $\mathbf{v} = [p, \mathbf{u}, \theta]$ is sought in the form:

$$\mathbf{v}(\chi, z, t) = \left(\mathbf{v}_0^{\mathrm{t}}(\chi, z) + \varepsilon^{1/2}\mathbf{v}_{1/2}^{\mathrm{t}}(\chi, z) + \varepsilon\mathbf{v}_1^{\mathrm{t}}(\chi, z) + \mathrm{O}(\varepsilon^{3/2})\right)\exp\left(\frac{\mathrm{i}}{\varepsilon^{1/2}}k^{\mathrm{t}}\chi - \mathrm{i}\omega_{\mathrm{G}}t\right), \tag{49}$$

with ω_{G} as in (34).

At leading order in ε, the local problem (24)–(26) at $X = 0$ is recovered. The leading order term $\mathbf{v}_0(\chi, z)$ is thus of the form:

$$\mathbf{v}_0^{\mathrm{t}}(\chi, z) = A(\chi)\hat{\mathbf{v}}_0^{\mathrm{t}}(z). \tag{50}$$

At the next order $\mathrm{O}(\varepsilon^{1/2})$, the inhomogeneous system

$$\mathcal{L}^{\mathrm{t}}[\partial_z]\mathbf{v}_{1/2}^{\mathrm{t}} = \mathcal{S}_{1/2}^{\mathrm{t}}\mathbf{v}_0^{\mathrm{t}} \tag{51}$$

is obtained where the vector $\mathcal{S}_{1/2}^{\mathrm{t}}\mathbf{v}_0^{\mathrm{t}}$ is given by

$$\mathcal{S}_{1/2}^{\mathrm{t}}\mathbf{v}_0^{\mathrm{t}} = \left[\partial_\chi A\left(\hat{\mathbf{u}}_0^{\mathrm{t}}\cdot\mathbf{e}_x\right), \partial_\chi A\left\{\left(2\mathrm{i}k^{\mathrm{t}} - R\tilde{U}_p\right)\hat{\mathbf{u}}_0^{\mathrm{t}} - \hat{p}_0^{\mathrm{t}}\mathbf{e}_x\right\}, \partial_\chi A\left(2\mathrm{i}k^{\mathrm{t}} - RP\tilde{U}_p\right)\hat{\theta}_0^{\mathrm{t}}\right]^{\mathrm{T}}. \tag{52}$$

At this order, the solvability condition is identically satisfied since $\partial_k\omega^{\mathrm{t}} = 0$ (see appendix D). The solution $\mathbf{v}_{1/2}^{\mathrm{t}} = (\mathbf{u}_{1/2}^{\mathrm{t}}, \theta_{1/2}^{\mathrm{t}}, p_{1/2}^{\mathrm{t}})$ is thus of the form:

$$\mathbf{v}_{1/2}^{\mathrm{t}} = \partial_\chi A\hat{\mathbf{v}}_{1/2}^{\mathrm{t}}. \tag{53}$$

Moreover, it is shown in appendix D how $\hat{\mathbf{v}}_{1/2}$ may be easily obtained from $\hat{\mathbf{v}}_0$. At the following order $\mathrm{O}(\varepsilon)$, one obtains:

$$\mathcal{L}^{\mathrm{t}}[\partial_z]\mathbf{v}_1^{\mathrm{t}} = \mathcal{S}_1^{\mathrm{t}}\left(\mathbf{v}_0^{\mathrm{t}}, \mathbf{v}_{1/2}^{\mathrm{t}}\right), \tag{54}$$

where $\mathcal{S}_1^{\mathrm{t}}(\mathbf{v}_0, \mathbf{v}_{1/2})$ is given by:

$$\begin{aligned}\mathcal{S}_1^{\mathrm{t}}(\mathbf{v}_0, \mathbf{v}_{1/2}) = \Bigg[&\partial_\chi^2 A\left(\hat{\mathbf{u}}_{1/2}^{\mathrm{t}}\cdot\mathbf{e}_x\right), \partial_\chi^2 A\left\{\hat{\mathbf{u}}_0^{\mathrm{t}} + (2\mathrm{i}k_{\mathrm{t}} - R\tilde{U}_p)\hat{\mathbf{u}}_{1/2}^{\mathrm{t}} - \hat{p}_{1/2}^{\mathrm{t}}\mathbf{e}_x\right\} + A\mathrm{i}P^{-1}\omega_1\hat{\mathbf{u}}_0^{\mathrm{t}},\\ &\partial_\chi^2 A\left\{\hat{\theta}_0^{\mathrm{t}} + (2\mathrm{i}k_{\mathrm{t}} - RP\tilde{U}_p)\hat{\theta}_{1/2}^{\mathrm{t}}\right\} + A\left\{\mathrm{i}\omega_1\hat{\theta}_0^{\mathrm{t}} + \frac{\chi^2}{2}\mathcal{R}''^{\mathrm{t}}\left(\hat{\mathbf{u}}_0^{\mathrm{t}}\cdot\mathbf{e}_z\right)\right\}\Bigg]^{\mathrm{T}}.\end{aligned} \tag{55}$$

Finally, the equation governing the global mode amplitude at this order is obtained by enforcing the solvability condition; using the coefficients α and β defined by (41) and (42), one obtains:

$$\partial_\chi^2 A - \left(\alpha\chi^2 + \beta\right)A = 0. \tag{56}$$

The detailed derivation of (56) is again given in appendix D.

Table I. Complex frequency correction ω_1 for different values of the Reynolds number R, P and $\mathcal{R}(X)$ as in *figure 2*.

R	$\mathcal{R}^{\mathrm{t}} = \mathcal{R}_{\mathrm{a}}$	k^{t}	ω^{t}	$\omega_1/(n+1/2)$
0	1707.76	3.116	0	−i2.502
0.1	1711.01	3.119 − i.1115	1.874	−.06967 − i2.549
0.2	1720.69	3.128 − i.2211	3.755	−.1417 − i2.685
0.5	1785.32	3.177 − i.5254	9.502	−.375 − i3.538
1	1987.67	3.274 − i.9302	19.57	−.6960 − i5.861
2	2617.51	3.368 − i1.461	41.09	−.4971 − i11.87
5	5551.16	3.225 − i2.185	107.6	4.771 − i30.80
10	13310.6	2.779 − i2.624	211.4	20.01 − i58.34

The general solution of (56) is

$$A = \varpi\left(\alpha^{1/2}\chi^2\right)\exp\left(-\alpha^{1/2}\chi^2/2\right), \tag{57}$$

where ϖ is a combination of a kind of hypergeometric functions (Kummer functions) M as:

$$\varpi(\zeta) = C_1 M(a, 1/2, \zeta) + C_2\zeta^{1/2} M(a+1/2, 3/2, \zeta), \tag{58}$$

as defined in Abramovitz and Stegun [16], C_1 and C_2 being two free constants. In (58) we use the coefficient a defined by (43) and ζ is an arbitrary complex variable. Determining the asymptotic behavior of A, as given by (57), for large χ, the asymptotic behavior (40) of the WKBJ solution can be recovered only when M reduces to Hermite polynomials [2]. This places a condition on a which must be such that $2a = -n$ with $n \in \mathbb{N}$. Finally, using the definition (43) of a, the following condition on the $\mathrm{O}(\varepsilon)$ correction of the global mode frequency, ω_1, is obtained:

$$\omega_1 = \partial_k^2\omega^{\mathrm{t}}\alpha^{1/2}\left(n+\frac{1}{2}\right), \tag{59}$$

recalling that $\alpha^{1/2}$ is uniquely defined by (41) and (44). As an illustration, we give in *table I* some typical values of the involved correction for various values of R at $P = 7$ and $\mathcal{R}(X)$ being a Gaussian with $\lim_{X\to\pm\infty}\mathcal{R}(X) = 1600 = \mathcal{R}_\infty$, $\mathcal{R}^{\mathrm{t}} = \mathcal{R}_{\mathrm{a}}$ and $\mathcal{R}'^{\mathrm{t}} = \mathcal{R}^{\mathrm{t}} - \mathcal{R}_\infty$, $\mathcal{R}_{\mathrm{a}}$ being obtained as in [14]. It is clear from inspection of the table, that $\Im(\omega_1)$ is always negative, corresponding to a stabilizing effect on the most amplified perturbation.

5. Results and discussion

The main result of the preceding sections is that the temporal evolution of global modes is entirely determined by the local flow properties at the location of maximum Rayleigh number $\mathcal{R}^{\mathrm{t}}$. Owing to the convective nature of the instability in the locally parallel flow at small supercritical Rayleigh numbers, time growth of linear global modes can only be obtained when $\mathcal{R}^{\mathrm{t}}$ is greater than the critical value for absolute instability $\mathcal{R}_{\mathrm{a}}$. For Reynolds numbers $R \geqslant \mathrm{O}(1)$, this implies an O(1) difference between the usual critical value $\mathcal{R}_{\mathrm{c}}^{(TR)}$ for transverse rolls (TR) in the parallel problem [17,13,18] and the critical value $\mathcal{R}_{\mathrm{G}}$ of the local Rayleigh number $\mathcal{R}^{\mathrm{t}}$ at $X = 0$ for global instability. In *figure 4*, this difference corresponds to the distance between the dashed and dot-dashed lines, representing the evolution of $\mathcal{R}_{\mathrm{c}}^{(TR)}$ and $\mathcal{R}_{\mathrm{a}}$, respectively, with R. The weakly non-parallel effects induce an additional smaller $\mathrm{O}(\varepsilon)$ frequency correction ω_1 (cf. equation (59)), with which the $\mathrm{O}(\varepsilon)$ approximation to

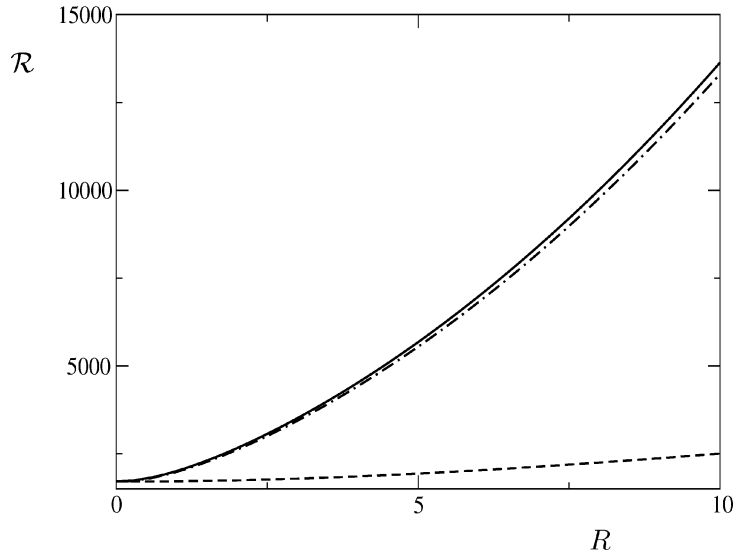

Figure 4. Critical value of the local Rayleigh number $\mathcal{R}^{\mathrm{t}} = \mathcal{R}(X = 0)$ for convective instability (dashed line), absolute instability (dot-dashed line) and global instability (solid line for $\varepsilon = 0.1$) as a function of the Reynolds number. $\mathcal{R}(X)$ and P as in *figure 2*.

$\mathcal{R}_{\mathrm{G}}$ is obtained from

$$\Im\left(\omega^{\mathrm{t}} + \varepsilon\omega_1\right) = 0. \tag{60}$$

Evidently, $\mathcal{R}_{\mathrm{G}}$ depends on all control parameters, as well as on the value of the small parameter ε. Since the $\mathrm{O}(\varepsilon)$ correction ω_1 is always found to have a negative imaginary part, $\mathcal{R}_{\mathrm{G}}$ always exceeds $\mathcal{R}_a$. This approximation of $\mathcal{R}_{\mathrm{G}}$ is shown as a solid line in *figure 4* for $\varepsilon = 0.1$ and the Gaussian Rayleigh number distribution $\mathcal{R}(X)$ defined in the caption of *figure 2*. It is first noted that $\mathcal{R}_{\mathrm{G}}$, like $\mathcal{R}_{\mathrm{a}}$ and $\mathcal{R}_{\mathrm{c}}^{(TR)}$, exhibits a very nearly quadratic dependence on R. To show the difference between the $\mathrm{O}(\varepsilon)$ approximation of $\mathcal{R}_{\mathrm{G}}$ and $\mathcal{R}_{\mathrm{a}}$ for different parameters, their relative difference is given in *figure 5* as a function or R for three values of ε spanning the typical values of interest. This relative difference is seen to first increase with R in the range $0 \leqslant R \leqslant 5$ and to reach a constant value for larger R. From an experimental standpoint, the difference between the critical Rayleigh numbers for convective and absolute instability should be clearly detectable for sufficiently large R, especially since this difference in Rayleigh numbers is associated with a marked frequency shift shown in *figure 6* (note that for non-zero Reynolds numbers, the transverse rolls under consideration are traveling waves). The $\mathrm{O}(\varepsilon)$ shift between global and absolute Rayleigh number, on the other hand, may be difficult to detect for small values of ε. Note that this shift subsists in the limiting Rayleigh–Bénard case, $R = 0$, and varies approximately linearly with ε for small ε in agreement with classical results (see e.g. [10]).

The value of the Prandtl number does not qualitatively affect the dependence of $\mathcal{R}_{\mathrm{G}}$ on R but, as is clear from *figure 7*, it has a strong quantitative effect. At large Prandtl numbers ($P = 450$ in *figure 7*), the value of $\mathcal{R}_{\mathrm{G}}$ increases very rapidly with R while it only slightly departs from the usual critical value $\mathcal{R}_{\mathrm{c}}^{(TR)}$ for transverse rolls (TR) in a spatially homogeneous (parallel) system at low P ($P = 0.71$ in 7).

Examples of the spatial structure of the most amplified global mode for three different Reynolds numbers are finally shown in *figure 8*, where the snapshots of isocontours of the normalized temperature perturbation $\theta_0(X, z)$ clearly display the streamwise variation of roll strength in relation to the imposed function $\mathcal{R}(X)$. From this figure it appears that, for any given value of R, the global modes analyzed in this paper consist of a 'roll-train' of approximately constant wavelength, smoothly modulated by a Gaussian-like envelope. In each

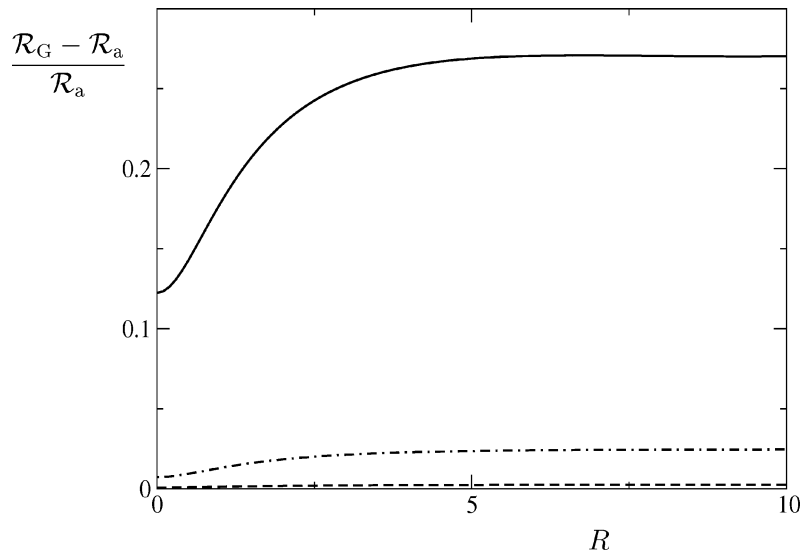

Figure 5. Relative difference between critical values of the Rayleigh number for global instability and local absolute instability at $X = 0$. $\varepsilon = 0.01$ (dashed line), 0.1 (dot-dashed line), 1 (solid line). $\mathcal{R}(X)$ and P as in *figure 2*.

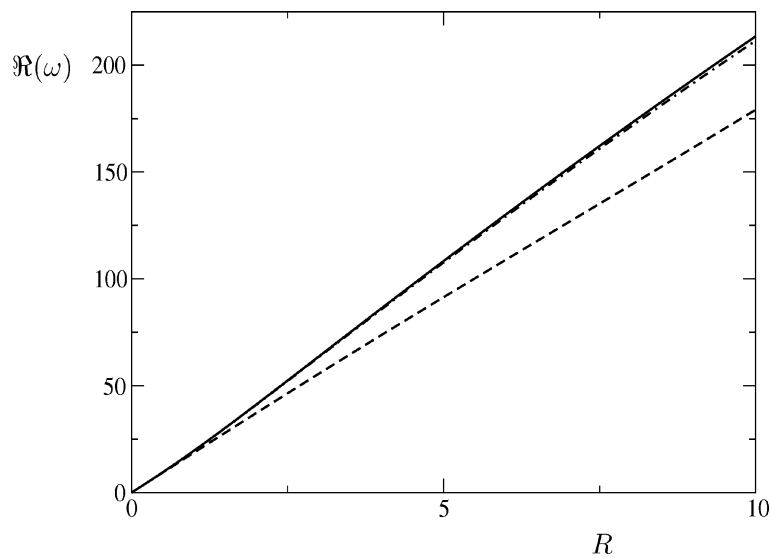

Figure 6. Real part of the frequency corresponding to the onset of convective instability (dashed line), absolute instability (dot-dashed line) and global instability (solid line for $\varepsilon = 0.1$) as a function of the Reynolds number. $\mathcal{R}(X)$ and P as in *figure 2*.

plot of $\mathcal{R}(X)$ the regions of local absolute $[-X_a, X_a]$ and convective $[-X_c, X_c]$ instability are indicated. As expected, the 'roll-train' reaches its maximum amplitude near X_c since, to leading WKBJ order, the downstream branch k^+ emerging from the turning point region at $X = 0$ is spatially amplified up to a point close to X_c (it is not exactly X_c, because the global frequency is close but not equal to the critical frequency at the convective stability boundary). As a consequence, depending on R and the location of X_c, rolls may be observed relatively far downstream of the location of maximum Rayleigh number and the ratio between peak roll amplitude and roll amplitude at $X^t = 0$ increases with X_c. The reader is however cautioned that the spatial structure of the

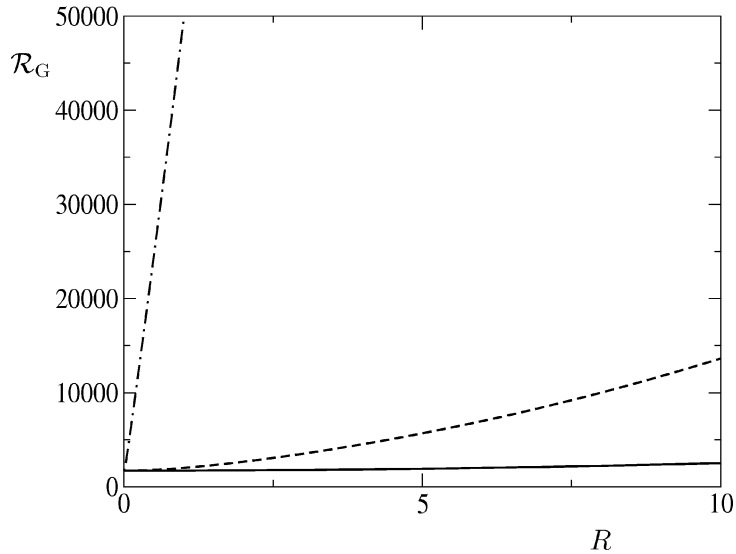

Figure 7. Critical value of the local Rayleigh number for global instability as a function of the Reynolds number for Prandtl number $P = 0.71$ (solid line), 7 (dashed line), 450 (dot-dashed line) and $\varepsilon = 0.1$. $\mathcal{R}(X)$ as in *figure 2*.

linear mode shown in *figure 8* is only relevant to the marginal case $\mathcal{R}^t \downarrow \mathcal{R}_G$, and this only if the bifurcation is supercritical. For larger $\mathcal{R}^t$, non-linearity is expected to affect the spatial structure, with rolls likely to progressively become stronger in the upstream region. In this context, we believe that the smooth shape of the envelope in *figure 8* should not be associated in a straightforward manner with the non-linearly saturated 'soft global modes' identified by Pier and Huerre [19]. The soft global modes require that $k^-(X)$ crosses the real k-axis, a condition which is not met here as the imaginary part of k^- is found to be negative for all X in the present case. In the case of a subcritical bifurcation, on the other hand, the structure shown in *figure 8* is likely to be irrelevant, since the slightest impulsive perturbation would probably result in the establishment of a nonlinear 'steep global modes' with a front located at $-X_a$, of the type analyzed by Pier et al. [20] in the context of the complex Ginzburg–Landau equation. Generally speaking, it may be difficult in the present system to experimentally distinguish between the two types of bifurcations since, due to the reality of X^t, the extent of the absolutely unstable region remains small of order $O(\varepsilon^{1/2})$.

Another question arising naturally concerns the relevance of the present purely two-dimensional approach (or one-dimensional in terms of wave propagation directions), in a system in which three-dimensional patterns (mainly longitudinal rolls) are commonly observed [21–28]. The longitudinal rolls in particular have been shown in our previous work [14] to be always convectively unstable, despite having a lower critical Rayleigh number $\mathcal{R}_c^{(LR)}$ than transverse rolls. Therefore, the experimental observation of the predicted global modes composed of transverse rolls will likely be restricted to facilities with very low external noise and limited streamwise extent, which allow to reach $\mathcal{R}_a > \mathcal{R}_c^{(LR)}$ while keeping the amplitude of the noise-driven longitudinal rolls below the observation threshold throughout the length of the cell. The situation does however not appear hopeless, since transverse rolls have been observed in several setups (see, for instance, [25] or [27]) at low Reynolds numbers and sufficiently large Rayleigh numbers. As already mentioned in the introduction, a future full analysis of a realistic (laboratory) system requires an extension of the present approach to spanwise inhomogeneities with the Rayleigh number depending on two slow coordinates X and Y. In addition, side-walls need to be introduced eventually. This opens the possibility of convection patterns other than rolls being dominant, as shown for instance by Rees [10] for the $R = 0$ case. Such an extension very seriously complicates the analysis to the point where the present two-dimensional case will be indispensable as 'anchoring point'.

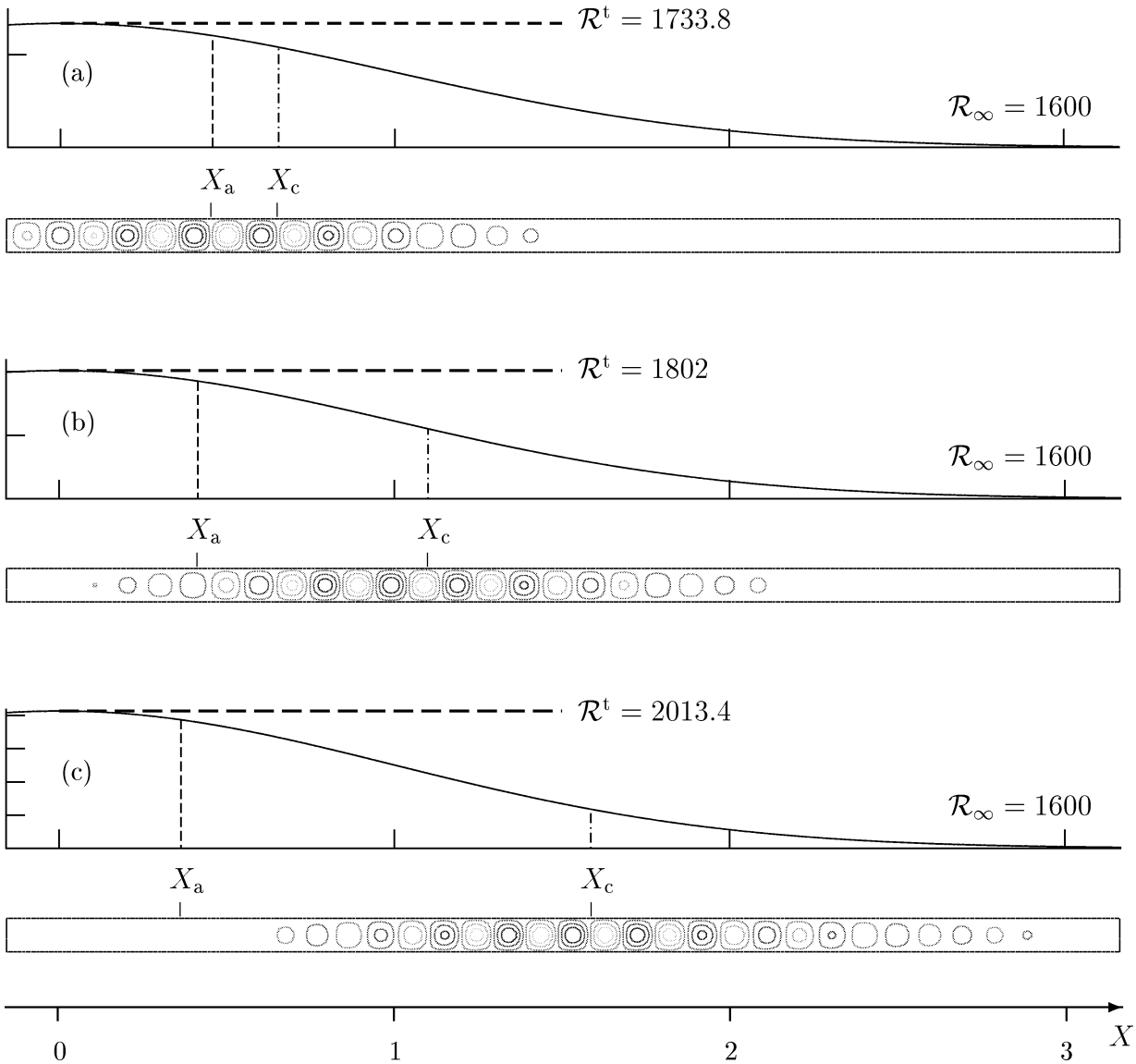

Figure 8. Isocontours of the temperature perturbation $\theta_0(X, z)$ corresponding to marginally stable global modes for three Reynolds numbers $R = 0.2$ (a), 0.5 (b), and 1 (c). Above each plot, the variation of the Rayleigh number with X is given, together with the regions of local absolute $[-X_\mathrm{a}, X_\mathrm{a}]$ and convective $[-X_\mathrm{c}, X_\mathrm{c}]$ instability. $\mathcal{R}(X)$ and P as in *figure 2* and $\varepsilon = 0.1$.

Acknowledgements

The authors are grateful to J.F. Scott and D. Martinand for several helpful discussions. The financial support of the Swiss National Science Foundation under grant no 21-39572.93 for the initial phase of the work, the ERCOFTAC Leonhard Euler Center and the Direction des Relations Internationales of the CNRS (Ph.C.) are also gratefully acknowledged.

A. Adjoint problem

The adjoint problem associated to the system of equation (24)–(26) is derived in a standard fashion. Introducing the inner product between $\hat{\mathbf{v}} = [\hat{p}, \hat{\mathbf{u}}, \hat{\theta}]$ and $\hat{\mathbf{v}}' = [\hat{p}', \hat{\mathbf{u}}', \hat{\theta}']$ as

$$\langle \hat{\mathbf{v}}, \hat{\mathbf{v}}' \rangle = \int_{-1/2}^{1/2} (\hat{p}\overline{\hat{p}'} + \hat{\mathbf{u}} \cdot \overline{\hat{\mathbf{u}}'} + \hat{\theta}\overline{\hat{\theta}'})\, \mathrm{d}z, \tag{61}$$

it is found that the governing equations for the adjoint mode $\hat{\mathbf{v}}_0^* = [\hat{p}_0^*, \hat{\mathbf{u}}_0^*, \hat{\theta}_0^*]$ are given by:

$$-\mathrm{i}\overline{k}(\hat{\mathbf{u}}_0^* \cdot \mathbf{e}_x) - \partial_z(\hat{\mathbf{u}}_0^* \cdot \mathbf{e}_z) = 0, \tag{62}$$

$$\mathrm{i}\overline{\omega} P^{-1}\hat{\mathbf{u}}_0^* - \mathrm{i}\overline{k} R\tilde{U}_p\hat{\mathbf{u}}_0^* + R\tilde{U}_p'(\hat{\mathbf{u}}_0^* \cdot \mathbf{e}_x)\mathbf{e}_z + (\mathrm{i}\overline{k}\mathbf{e}_x + \mathbf{e}_z\partial_z)\hat{p}_0^* - \mathcal{R}\hat{\theta}_0^*\mathbf{e}_z + (\overline{k}^2 - \partial_z^2)\hat{\mathbf{u}}_0^* = 0, \tag{63}$$

$$\mathrm{i}\overline{\omega}\hat{\theta}_0^* - \mathrm{i}\overline{k} RP\tilde{U}_p\hat{\theta}_0^* - (\hat{\mathbf{u}}_0^* \cdot \mathbf{e}_z) + (\overline{k}^2 - \partial_z^2)\hat{\theta}_0^* = 0, \tag{64}$$

which defines $\mathcal{L}^*$, the adjoint operator to $\mathcal{L}$ defined by (27).

B. Coefficients of the WKBJ amplitude equation

The coefficients of the WKBJ amplitude equation (37) may be conveniently expressed using formal derivatives of the linear operator $\mathcal{L}$ defined by (27). The existence of non trivial solutions $\hat{\mathbf{v}}_0$ of (27) requires that k, ω and X are related through the dispersion relation (28). Formally deriving (27), one can alternatively use any pair of these three variables as independent: this is possible with the exception of singular points of the dispersion relation (for instance when $\partial_k\omega = 0$ or $\partial_X\omega = 0$) which whatever correspond to the breakdown of the WKBJ approximation where consequently (37) does not hold.

Of particular interest are the first- and second-order derivatives of $\mathcal{L}$ with respect to k at constant X:

$$\partial_k\mathcal{L}|_X = \begin{pmatrix} 0 & -\mathrm{i}(\mathbf{e}_x\cdot) & 0 \\ \mathrm{i}\mathbf{e}_x & (-\mathrm{i}\partial_k\omega P^{-1} + \mathrm{i}R\tilde{U}_p + 2k)\mathbf{I} & 0 \\ 0 & 0 & -\mathrm{i}\partial_k\omega + \mathrm{i}RP\tilde{U}_p + 2k \end{pmatrix}, \tag{65}$$

$$\partial_k^2\mathcal{L}|_X = \begin{pmatrix} 0 & 0 & 0 \\ 0 & (-\mathrm{i}\partial_k^2\omega P^{-1} + 2)\mathbf{I} & 0 \\ 0 & 0 & -\mathrm{i}\partial_k^2\omega + 2 \end{pmatrix}, \tag{66}$$

where $\mathbf{I}$ denotes the identity operator in $\mathbb{R}^3$. Now, derivation of (27) with respect to k at constant X gives:

$$\partial_k\mathcal{L}|_X\hat{\mathbf{v}}_0 = -\mathcal{L}\partial_k\hat{\mathbf{v}}_0|_X, \tag{67}$$

which, using the inner product with the adjoint mode $\hat{\mathbf{v}}_0^*$, leads to the following property of $\partial_k\mathcal{L}$:

$$\begin{aligned} \langle \partial_k\mathcal{L}|_X\hat{\mathbf{v}}_0, \hat{\mathbf{v}}_0^* \rangle &= -\langle \mathcal{L}\partial_k\hat{\mathbf{v}}_0|_X, \hat{\mathbf{v}}_0^* \rangle \\ &= -\langle \partial_k\hat{\mathbf{v}}_0|_X, \mathcal{L}^*\hat{\mathbf{v}}_0^* \rangle \\ &= 0. \end{aligned} \tag{68}$$

Similarly, one derives the following property for $\partial_k^2\mathcal{L}$:

$$\langle \partial_k^2\mathcal{L}|_X\hat{\mathbf{v}}_0, \hat{\mathbf{v}}_0^*\rangle + \langle \partial_k\mathcal{L}|_X\partial_k\hat{\mathbf{v}}_0|_X, \hat{\mathbf{v}}_0^*\rangle = 0. \tag{69}$$

Also, we introduce the linear operators $\mathcal{I}_P$ as:

$$\mathcal{I}_P = \begin{pmatrix} 0 & 0 & 0 \\ 0 & P^{-1}\mathbf{I} & 0 \\ 0 & 0 & 1 \end{pmatrix}. \tag{70}$$

Since the pressure terms may always be eliminated from the original equations, one can use:

$$\langle \mathcal{I}_P\hat{\mathbf{v}}_0, \hat{\mathbf{v}}_0^*\rangle = 1, \tag{71}$$

as the normalization for $\hat{\mathbf{v}}_0$. Note also that $\partial_k\hat{\mathbf{v}}_0|_X$ being defined via (67), it is known up to an arbitrary value in the direction of $\hat{\mathbf{v}}_0$. Thus, it may be imposed that:

$$\langle \mathcal{I}_P\partial_k\hat{\mathbf{v}}_0|_X, \hat{\mathbf{v}}_0^*\rangle = 0, \tag{72}$$

so as $\partial_k\hat{\mathbf{v}}_0|_X$ to be uniquely defined. Such a normalization has to be used whatever is the partial derivative which is involved so that, for instance:

$$\langle \mathcal{I}_P\partial_\omega\hat{\mathbf{v}}_0|_k, \hat{\mathbf{v}}_0^*\rangle = 0. \tag{73}$$

Finally, introducing $\mathcal{L}_\varepsilon$, which refers to the $O(\varepsilon)$ correction of the base flow, as:

$$\mathcal{L}_\varepsilon = \begin{pmatrix} 0 & 0 & 0 \\ 0 & P^{-1}(\mathrm{i}k\tilde{U}_1 + \tilde{U}_1'(\mathbf{e}_z\cdot)\mathbf{e}_x)\mathbf{I} & 0 \\ 0 & \tilde{T}_0(\mathbf{e}_x\cdot) + \tilde{T}_1'(\mathbf{e}_z\cdot) & \mathrm{i}k\tilde{U}_1 \end{pmatrix}, \tag{74}$$

and recalling that the WKBJ expansion has been performed considering ω and X as independent variables, one obtains the following alternative expression for the right-hand side term of equation (35):

$$\begin{aligned}\mathcal{S}_1\hat{\mathbf{v}}_0^\pm = \partial_X A^\pm\big(\mathrm{i}\partial_k\mathcal{L}^\pm|_X - \partial_k\omega^\pm\mathcal{I}_P\big)\hat{\mathbf{v}}_0^\pm + A^\pm(X)\Bigg[\Bigg(\mathrm{i}\omega_1\mathcal{I}_P + \frac{\mathrm{i}}{2}\partial_X k^\pm\partial_k^2\mathcal{L}^\pm|_X \\ -\frac{1}{2}\partial_X k^\pm\partial_k^2\omega^\pm\mathcal{I}_P\Bigg)\hat{\mathbf{v}}_0^\pm + \big(\mathrm{i}\partial_k\mathcal{L}^\pm|_X - \partial_k\omega^\pm\mathcal{I}_P\big)\partial_X\hat{\mathbf{v}}_0^\pm|_\omega - \mathcal{R}'(X)\mathcal{L}_\varepsilon^\pm\hat{\mathbf{v}}_0^\pm\Bigg].\end{aligned} \tag{75}$$

Solvability condition for solving (35) requires that $\langle\mathcal{S}_1\hat{\mathbf{v}}_0^\pm, \hat{\mathbf{v}}_0^{*\pm}\rangle = 0$. For further simplifications in the expressions of the coefficient, we first use, in equation (75), the identity:

$$\partial_X\hat{\mathbf{v}}_0|_\omega = \partial_X k\partial_k\hat{\mathbf{v}}_0|_X + \partial_X\omega\partial_\omega\hat{\mathbf{v}}_0|_k. \tag{76}$$

Replacing $\mathcal{S}_1^\pm\hat{\mathbf{v}}_0$ by its expression as in (75), using (76) and further simplifying using (68)–(72) and (73), the solvability condition becomes:

$$\begin{aligned}\partial_k\omega^\pm\partial_X A^\pm + A^\pm(X)\Bigg[-\mathrm{i}\omega_1 + \frac{1}{2}\partial_X^\pm k\partial_k^2\omega^\pm - \mathrm{i}\partial_X\omega^\pm\langle\,\partial_k\mathcal{L}^\pm|_X\partial_\omega\hat{\mathbf{v}}_0^\pm|_k, \hat{\mathbf{v}}_0^{*\pm}\rangle \\ + \mathcal{R}'(X)\langle\mathcal{L}_\varepsilon^\pm\hat{\mathbf{v}}_0^\pm, \hat{\mathbf{v}}_0^{*\pm}\rangle\Bigg] = 0,\end{aligned} \tag{77}$$

so that the coefficients involved in (37) are given by:

$$\eta_{k\omega}^{\pm} = -\mathrm{i}\langle \partial_k \mathcal{L}^{\pm}|_X \partial_\omega \hat{\mathbf{v}}_0^{\pm}|_k, \hat{\mathbf{v}}_0^{*\pm}\rangle, \tag{78}$$

$$\eta_{\varepsilon}^{\pm} = \langle \mathcal{L}_{\varepsilon}^{\pm} \hat{\mathbf{v}}_0^{\pm}, \hat{\mathbf{v}}_0^{*\pm}\rangle. \tag{79}$$

Finally, introducing the operator:

$$\mathcal{J}_\theta = \begin{pmatrix} 0 & 0 & 0 \\ 0 & 0 & 0 \\ 0 & (\mathbf{e}_z \cdot) & 0 \end{pmatrix}, \tag{80}$$

it is easily obtained that:

$$\partial_X \mathcal{L}|_k = -\mathrm{i}\partial_X \omega \mathcal{I}_P + \mathcal{R}'(X)\mathcal{J}_\theta. \tag{81}$$

Since $\partial_X \mathcal{L}|_k$ also satisfies the property:

$$\langle \partial_X \mathcal{L}|_k \hat{\mathbf{v}}_0, \hat{\mathbf{v}}_0^*\rangle = 0, \tag{82}$$

it follows that:

$$\partial_X \omega = -\mathrm{i}\mathcal{R}'(X)\langle \mathcal{J}_\theta \hat{\mathbf{v}}_0, \hat{\mathbf{v}}_0^*\rangle. \tag{83}$$

Formally introducing the partial derivative with respect to $\mathcal{R}$ (at constant k), one may equivalently writes:

$$\partial_{\mathcal{R}} \omega = -\mathrm{i}\langle \mathcal{J}_\theta \hat{\mathbf{v}}_0, \hat{\mathbf{v}}_0^*\rangle. \tag{84}$$

C. Asymptotic expansion of the WKBJ solution for $X \to 0$

Asymptotic expansion of (38) requires to determine the behavior of the k^- and k^+ branches as $X = 0$ is approached. The Taylor expansion [2] of ω in the vicinity of $X = 0$ reduces to:

$$\omega(k, X) = \omega^{\mathrm{t}} + \frac{1}{2}\partial_k^2 \omega^{\mathrm{t}} \left(k - k^{\mathrm{t}}\right)^2 + \frac{1}{2}\partial_X^2 \omega^{\mathrm{t}} X^2 + \mathrm{O}_3, \tag{85}$$

since $\partial_k \omega^{\mathrm{t}} = 0$ and $\partial_X \omega^{\mathrm{t}} = 0$ at the double turning point, and $\partial_{k,X}^2 \omega^{\mathrm{t}} = 0$ is also satisfied because $\partial_X \omega^{\mathrm{t}}$ is directly related to $\mathcal{R}'^{\mathrm{t}}$ via (32) which vanishes whatever is the value of k. As $\omega(k, X) = \omega^{\mathrm{t}}$ along a branch, and introducing the inner variable χ, it follows that:

$$k = k^{\mathrm{t}} \pm \varepsilon^{1/2} \mathrm{i}\alpha^{1/2}|\chi| + \mathrm{O}(\varepsilon), \tag{86}$$

recalling that $\alpha^{1/2}$ has been chosen so as to have a positive real part. The conversion from k^- for $\chi < 0$ to k^+ for $\chi > 0$ is thus given by:

$$k^{\pm} = k^{\mathrm{t}} + \varepsilon^{1/2} \mathrm{i}\alpha^{1/2}\chi + \mathrm{O}(\varepsilon). \tag{87}$$

Using (87) in the exponential term of (38) leads to:

$$\exp\left(\frac{\mathrm{i}}{\varepsilon}\int_0^X k^{\pm}(\omega^{\mathrm{t}}, X)\,\mathrm{d}X\right) = \exp\left(\mathrm{i}k_{\mathrm{t}}\frac{\chi}{\varepsilon^{1/2}} - \alpha^{1/2}\frac{\chi^2}{2}\right) + \mathrm{O}\left(\varepsilon^{1/2}\right). \tag{88}$$

[2] Formally, the relevance of such a Taylor expansion requires that $\partial_\omega D \neq 0$, where D is the dispersion relation yet defined and the partial derivative being taken at constant k and X. This was always found to be satisfied in our present investigations.

From (87) it follows that:

$$\partial_X k^{\pm t} = i\alpha^{1/2} + O(\varepsilon^{1/2}). \tag{89}$$

Also, since $\mathcal{R}'^{t} = 0$, one has:

$$\mathcal{R}(\chi) = O(\varepsilon^{1/2}), \tag{90}$$

and consequently:

$$\partial_X \omega = O(\varepsilon^{1/2}) \quad \text{for small } X. \tag{91}$$

Finally, expanding $\partial_k \omega$ around $X = 0$ for $\omega = \omega^t$, taking into account that $\partial_k \omega^t = 0$ and $\partial^2_{k,X}\omega^t = 0$ and using (87) it is obtained that:

$$\partial_k \omega = \varepsilon^{1/2} i\alpha^{1/2} \partial_k^2 \omega^t \chi + O(\varepsilon). \tag{92}$$

It thus follows that:

$$\ln A^{\pm} = -\frac{1}{2}\left(1 + \frac{\beta}{\alpha^{1/2}}\right) \int \chi^{-1}\, d\chi + O(\varepsilon^{1/2}), \tag{93}$$

with β as defined by (42), the integration of which leads to the asymptotic expression (40) given in the text.

D. Coefficient of amplitude equation in the double turning point region

From appendix B, it is immediately obtained that the right-hand side term $\mathcal{S}^t_{1/2}\mathbf{v}^t_0$ of equation (51) may be written as:

$$\mathcal{S}^t_{1/2}\mathbf{v}^t_0 = \partial_\chi A i\partial_k \mathcal{L}|^t_X \hat{\mathbf{v}}^t_0, \tag{94}$$

since $\partial_k \omega^t = 0$. From (68) it follows that:

$$\langle \mathcal{S}^t_{1/2}\hat{\mathbf{v}}^t_0, \hat{\mathbf{v}}^{*t}_0 \rangle = 0, \tag{95}$$

so that the compatibility condition is identically satisfied. Also, using the equality (67), equation (51) may be expressed as:

$$\mathcal{L}^t \mathbf{v}^t_{1/2} = -i\partial_\chi A \mathcal{L}^t \partial_k \hat{\mathbf{v}}_0|^t_X, \tag{96}$$

from which it is obtained that:

$$\hat{\mathbf{v}}^t_{1/2} = -i\partial_k \hat{\mathbf{v}}_0|^t_X. \tag{97}$$

Similarly, the right-hand side term $\mathcal{S}^t_1(\mathbf{v}^t_0, \mathbf{v}^t_{1/2})$ of equation (54) may be expressed as:

$$\mathcal{S}^t_1(\mathbf{v}^t_0, \mathbf{v}^t_{1/2}) = \partial^2_X A\left[\left(\frac{1}{2}\partial^2_k \mathcal{L}|^t_X + i\partial^2_k \omega^t \mathcal{I}_P\right)\hat{\mathbf{v}}^t_0 + i\partial_k \mathcal{L}|^t_X \mathbf{v}^t_{1/2}\right] + A\left(i\omega_1 \mathcal{I}_P + \frac{\chi^2}{2}\mathcal{R}''^t \mathcal{J}_\theta\right)\hat{\mathbf{v}}^t_0. \tag{98}$$

Using (69) and (71) and the identification (97) of $\mathbf{v}^t_{1/2}$, the compatibility condition reads:

$$i\partial^2_k \omega^t \partial^2_X A + A\left[i\omega_1 + \frac{\chi^2}{2}\mathcal{R}''^t \langle \mathcal{J}_\theta \hat{\mathbf{v}}^t_0, \hat{\mathbf{v}}^{*t}_0 \rangle\right] = 0. \tag{99}$$

Further simplification is obtained remarking that, since $\mathcal{R}'^t = 0$, one has:

$$\partial^2_X \omega^t = \partial_{\mathcal{R}} \omega^t \mathcal{R}''^t, \tag{100}$$

which using (84) leads to the expression:

$$\frac{1}{2}\partial_k^2\omega_0^{\mathrm{t}}\partial_\chi^2 A + A\left(\omega_1 - \frac{\chi^2}{2}\partial_X^2\omega_0^{\mathrm{t}}\right) = 0. \tag{101}$$

Using the coefficients α and β as defined by (41) and (42), equation (56) is easily obtained.

References

[1] Pierrehumbert R.T., Local and global baroclinic instability of zonally varying flows, J. Atmos. Sci. 41 (1984) 2141–2162.
[2] Huerre P., Monkewitz P.A., Local and global instabilities in spatially developing flows, Annu. Rev. Fluid Mech. 22 (1990) 473–537.
[3] Le Dizès S., Huerre P., Chomaz J.-M., Monkewitz P.A., Linear global modes in spatially developing media, Philos. T. Roy. Soc. A 354 (1996) 169–212.
[4] Yakubenko P.A., Global capillary instability of an inclined jet, J. Fluid Mech. 346 (1997) 181–200.
[5] Chomaz J.-M., Huerre P., Redekopp L.G., A frequency selection criterion in spatially developing flows, Stud. Appl. Math. 84 (1991) 119–144.
[6] Chomaz J.-M., Huerre P., Redekopp L.G., Bifurcation to local and global modes in spatially developing flows, Phys. Rev. Lett. 60 (1988) 25–28.
[7] Soward A.M., Jones C.A., The linear stability of the flow in the narrow gap between two concentric rotating spheres, Q. J. Mech. Appl. Math. 36 (1) (1983) 19–42.
[8] Monkewitz P.A., Huerre P., Chomaz J.-M., Global linear stability analysis of weakly non-parallel shear flows, J. Fluid Mech. 251 (1993) 1–20.
[9] Walton I.C., On the onset of Rayleigh–Bénard convection in a fluid layer of slowly increasing depth, Stud. Appl. Math. 67 (1982) 199–216.
[10] Rees D.A.S., The effect of long-wavelength thermal modulations on the onset of convection in an infinite porous layer heated from below, Q. J. Mech. Appl. Math. 43 (1990) 189–214.
[11] Walton I.C., The effect of a shear flow on convection in a layer heated non-uniformly from below, J. Fluid Mech. 154 (1985) 303–319.
[12] Hunt R.E., Crighton D.G., Instability of flows in spatialy developing media, P. Roy. Soc. A 435 (1991) 109–129.
[13] Müller H.W., Lücke M., Kamps M., Transversal convection patterns in horizontal shear flow, Phys. Rev. A 45 (1992) 3714–3726.
[14] Carrière Ph., Monkewitz P.A., Convective versus absolute instabilities in mixed Rayleigh–Bénard–Poiseuille convection, J. Fluid Mech. 384 (1999) 243–262.
[15] Crighton D.G., Gaster M., Stability of slowly diverging jet flow, J. Fluid Mech. 77 (1976) 397–413.
[16] Abramovitz M., Stegun I.A., Handbook of Mathematical Functions with Formulas, Graphs and Mathematical Tables, National Bureau of Standards, 1964.
[17] Gage K.S., Reid W.H., The stability of thermally stratified plane Poiseuille flow, J. Fluid Mech. 33 (1968) 21–32.
[18] Fujimura K., Kelly R.E., Interaction between longitudinal convection rolls and transverse waves in unstably stratified plane Poiseuille flow, Phys. Fluids 7 (1) (1995) 68–79.
[19] Pier B., Huerre P., Fully nonlinear global modes in spatially developing media, Physica D 97 (1996) 206–222.
[20] Pier B., Huerre P., Chomaz J.-M., Couairon A., Steep nonlinear global modes in spatially developing media, Phys. Fluids 10 (1998) 2433–2435.
[21] Akiyama M., Hwang G.J., Cheng K.C., Experiments on the onset of longitudinal vortices in laminar forced convection between horizontal plates, J. Heat Transfer 93 (1971) 335–341.
[22] Ostrach S., Kamotani Y., Heat transfer augmentation in laminar fully developed channel flow by means of heating from below, J. Heat Trans-T ASME 97 (1975) 220–225.
[23] Luijkx J.M., Platten J.K., Legros J.-Cl., On the existence of thermoconvective rolls, transverse to a superimposed mean Poiseuille flow, Int. J. Heat Mass Tran. 24 (7) (1981) 1287–1291.
[24] Fukui K., Nakajima M., Hueda H., The longitudinal vortex and its effects on the transport processes in combined free and forced laminar convection between horizontal and inclined parallel plates, Int. J. Heat Mass Tran. 26 (1) (1983) 109–120.
[25] Ouazzani M.T., Catalgirone J.P., Meyer G., Mojtabi A., Etude numérique et expérimentale de la convection mixte entre deux plans horizontaux à températures différentes, Int. J. Heat Mass Tran. 32 (2) (1989) 261–269.
[26] Ouazzani M.T., Platten J.K., Mojtabi A., Etude numérique et expérimentale de la convection mixte entre deux plans horizontaux à températures différentes – II, Int. J. Heat Mass Tran. 33 (7) (1990) 1417–1427.
[27] Yu C.H., Chang M.Y., Lin T.F., Structures of moving transverse and mixed rolls in mixed convection of air in a horizontal plane channel, Int. J. Heat Mass Tran. 40 (2) (1997) 333–346.
[28] Chang M.Y., Yu C.H., Lin T.F., Changes of longitudinal vortex roll structure in a mixed convective air flow through a horizontal plane channel: an experimental study, Int. J. Heat Mass Tran. 40 (2) (1997) 347–363.